

Article

Unraveling the Relationship between Microstructure and Mechanical Properties of Friction Stir-Welded Copper Joints by Fuzzy Logic Neural Networks

Mousa Javidani ^{1,*}, Akbar Heidarzadeh ^{2,*}, Reza Vatankhah Barenji ³, Moslem Paidar ⁴ and Hamid Reza Jafarian ⁵

¹ Department of Applied Science, University of Québec at Chicoutimi, Saguenay, QC G7H 2B1, Canada

² Department of Materials Engineering, Azarbaijan Shahid Madani University, Tabriz 5375171379, Iran

³ Department of Engineering, School of Science and Technology, Nottingham Trent University, Nottingham NG11 8NS, UK; reza.vatankhahbarenji@ntu.ac.uk

⁴ Department of Material Engineering, South Tehran Branch, Islamic Azad University, Tehran 1459853849, Iran; m.paidar@srbiau.ac.ir

⁵ School of Metallurgy and Materials Engineering, Iran University of Science and Technology, Narmak, Tehran 1311416846, Iran; jafarian@iust.ac.ir

* Correspondence: mousa_javidani@uqac.ca (M.J.); ac.heydarzadeh@azaruniv.ac.ir (A.H.)

Abstract: In this study, fuzzy logic neural networks were employed to optimize the friction stir welding (FSW) process parameters in the joining of copper plates. The FSW parameters were considered as the input variables, for which micro-hardness, nano-hardness, and yield strength of the joints were the responses. The micro-hardness and nano-hardness were measured by Vickers hardness and nanoindentation tests, respectively. The microstructure and substructure of the joints were evaluated by optical, scanning electron, and orientation imaging microscopes. The optimum process parameters through which the maximum strength was achieved were the tool rotational rate of 560 rpm, tool traverse speed of 175 mm/min, and tool axial force of 2.27 kN. The low heat input joints, owing to the finer grain sizes, high density of dislocations, and larger Taylor factors, indicated greater strength relative to the high input joints. Microstructure characterization revealed that dominant strengthening mechanisms of the joints were dislocation density, texture effect, and grain boundary hardening.

Keywords: FSW; fuzzy model; microstructural evolution; hardness



Citation: Javidani, M.; Heidarzadeh, A.; Vatankhah Barenji, R.; Paidar, M.; Jafarian, H.R. Unraveling the Relationship between Microstructure and Mechanical Properties of Friction Stir-Welded Copper Joints by Fuzzy Logic Neural Networks. *Crystals* **2022**, *12*, 216. <https://doi.org/10.3390/cryst12020216>

Academic Editor: Bolv Xiao

Received: 11 January 2022

Accepted: 29 January 2022

Published: 31 January 2022

Publisher's Note: MDPI stays neutral with regard to jurisdictional claims in published maps and institutional affiliations.



Copyright: © 2022 by the authors. Licensee MDPI, Basel, Switzerland. This article is an open access article distributed under the terms and conditions of the Creative Commons Attribution (CC BY) license (<https://creativecommons.org/licenses/by/4.0/>).

1. Introduction

Copper and copper alloys have attracted attention due to their distinctive characteristics, such as high mechanical strength and excellent electrical conductivity. Owing to their face-centered cube (FCC) crystallographic structure, they also present high formability, which makes them suitable in the production of various final shapes such as plates, profiles, tubes, bars, etc [1]. On the other hand, thanks to its single-phase structure, copper is usually used as a material for fundamental research investigations [2]. Consequently, due to these unique characteristics, there is a surging demand for joining copper and copper alloys.

During fusion welding of copper and copper alloy, very high heat input is required owing to their intrinsic high thermal conductivity. The required high input can lead to several welding defects, such as oxidation, color change, evaporation of elements such as zinc in brass alloys, etc. In addition, high heat inputs cause a wider heat-affected zone (HAZ), through which the microstructure and mechanical properties can be deteriorated [3]. Consequently, as fusion welding has not been appreciated for copper, new methods with lower heat inputs (e.g., solid-state techniques) have recently been developed to join copper plates [4].

Friction stir welding (FSW), schematically shown in Figure 1, is a solid-state joining process. Even though FSW was initially developed for the welding of Al alloys in 1991 [5], it has been successfully employed in the joining of copper and copper alloys [6]. During FSW, the base metals (BMs) are clamped by a fixture on a milling machine. A rotational tool enters the interfaces between the BMs and moves along the joining line. As BMs do not experience fusion, most of the common disadvantages of fusion welding processes (e.g., oxidation, porosities, shrinkages, cracking, etc.) can be eliminated by FSW. The joining mechanism by FSW is through applied severe plastic deformation (SPD) [5]. The rotating tool of FSW is composed of a pin and a shoulder. The pin applies the plastic deformation to the BMs whereas the main role of the shoulder is generating heat through the friction produced between the shoulder and the BMs' surfaces. As material deformation is carried out at a relatively high temperature, FSW is considered a thermomechanical process. Therefore, the deformation restoration mechanisms, such as dynamic recovery (DRV) and dynamic recrystallization (DRX), can be activated during FSW [5].

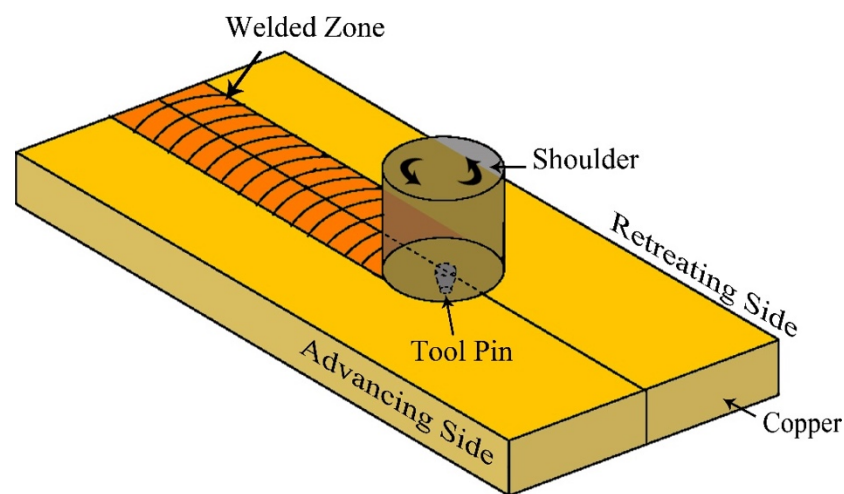


Figure 1. Schematic of friction stir welding process.

Several research studies have been conducted to obtain high-strength, defect-free joints by optimizing the FSW parameters. Ramesh Babu et al. [7] employed the Taguchi method to study the FSW of Al alloys containing SiC particles. Kumar et al. [8] investigated the FSW of AA6101-T6 alloys. Shunmugasundaram et al. [9] used FSW to join dissimilar AA6063 and AA5052 aluminum alloys, and they studied the effect of different parameters on the final properties. Dhabale et al. [10] examined the submerged FSW of Al6061-6063 aluminum alloy using the Taguchi method. Ramesh et al. [11] used the Taguchi technique to explore the dissimilar FSW joining of AA5083 and AA6061 Al alloys. Heidarzadeh et al. [12] studied the submerged, dissimilar FSW of AA6061 and AA7075 Al alloys. Senthil et al. [13] employed the response surface method (RSM) to optimize the FSW of 6063-T6 pipes using a multi-objective process. Sasikumar et al. [14] predicted the tensile strength of dissimilar AA6082/AA5052 FSWed plates using RSM. In another study, the joint formation mechanism was studied by a numerical model of plastic flow combined with experimental approaches [15]. A fluid–solid interaction algorithm was proposed to establish the coupling model, and the welding material was treated as a non-Newtonian fluid [15]. A high-throughput screening method, based on the relation between massively parallel computational methods and an existing database containing the calculated properties, is capable of exploring hypothetical candidates [16].

The use of the fuzzy logic method in optimizing the FSW parameters, especially in the case of pure copper, has been scarcely reported. Most recently, Heidarzadeh et al. [17] successfully employed the fuzzy logic model to predict tensile properties and optimize the process parameters in the case of the FSWed pure copper joints. Fuzzy logic models were proven to be more suitable for process optimization relative to other modeling ap-

proaches [18]. Therefore, in this study, the hardness and yield strength of FSWed copper joints were predicted, and the FSW process parameters were optimized by employing the fuzzy logic model [17]. In addition, the dominant strengthening mechanisms at various FSW conditions (i.e., different heat inputs) were identified using orientation image microscopy (OIM) and transmission electron microscopy (TEM).

2. Experimental Procedure

The experimental design, conducted by Design-Expert software, was based on the central composite rotatable design (CCRD) method. The levels of parameters and the experimental design matrix are shown in Tables 1 and 2, respectively. The details of the experimental procedure as well as the details of fuzzy logic modeling, which have been presented with detail in our recently published paper [17], are omitted here for the sake of brevity.

The base metals (BMs), i.e., copper plates, had 150 mm length \times 100 mm width \times 2 mm thick dimensions. The commercially pure copper plates were annealed at 500 °C for 1 h and had a single-phase microstructure, and they were joined using an H13 FSW tool. The tool had a cylindrical shoulder (of 12 mm diameter) and a simple cylindrical pin (of 3 mm diameter and 1.7 mm length). Moreover, the tilt angle of the tool relative to the normal direction of the plate surface was set constant at 2.5°, and the plates were supported during FSW by a steel backing plate. The samples for microstructure characterization were cut from the stir zone (SZ), mounted, and subjected to the standard grinding and polishing procedure. The microstructures were studied by optical microscopy (OM), an electron backscattered diffraction (EBSD) system, and a scanning transmission electron microscope (STEM, Hitachi S-4800). The hardness of the joints at the middle of SZ was measured using Vickers hardness tester by applying 50 gr load and indentation time of 10 s. Nanoindentation was also used to measure the nanomechanical properties for which 20 experiments were conducted per joint. In addition, the yield strength values were extracted from the nanoindentation results using a method established by Dao et al. [19]. For each joint, the hardness of joints (SZ) was measured 20 times, and the average amount was reported.

Table 1. The parameters and their levels used in this study, according to the CCRD method.

Parameters	Unit	Levels				
		−1.68	−1	0	1	1.68
Rotational speed (A)	rpm	463	600	800	1000	1136
Traverse speed (B)	mm/min	16	50	100	150	184
Axial force (C)	kN	1.66	2	2.5	3	3.34

Table 2. Experimental design matrix used in this study.

Run	Rotational Speed (rpm)	Traverse Speed (mm/min)	Axial Force (kN)
1	600	50	2
2	1000	50	2
3	600	150	2
4	1000	150	2
5	600	50	3
6	1000	50	3
7	600	150	3
8	1000	150	3
9	463	100	2.5

Table 2. Cont.

Run	Rotational Speed (rpm)	Traverse Speed (mm/min)	Axial Force (kN)
10	1136	100	2.5
11	800	16	2.5
12	800	184	2.5
13	800	100	1.66
14	800	100	3.34
15	800	100	2.5
16	800	100	2.5
17	800	100	2.5
18	800	100	2.5
19	800	100	2.5
20	800	100	2.5

3. Results

The Fuzzy Logic Toolbox in Matlab R2013a software was used for solving the fuzzy inference system (FIS). The definition stated in Equation (1) was used for defuzzification.

$$x^* = \frac{\sum_{i=1}^n x_i \cdot \mu(x_i)}{\sum_{i=1}^n \mu(x_i)} \quad (1)$$

where x^* is the defuzzified values of the hardness and yield strength, x_i stands for the centroid of the area, $\mu(x_i)$ refers to the firing step of the i th rule, and n mentions the whole number of rules fired. The micro-hardness, nano-hardness, and yield strength profiles of the samples are shown in Figures 2–4. Comparing the defuzzified outputs with the experimental results, as shown in Figures 2–4 and Table 3, indicates that the outputs were accurately predicted by the FIS. It can be concluded that, in cases where crisp values of inputs are not available or hard to achieve, fuzzy models can offer accurate results.

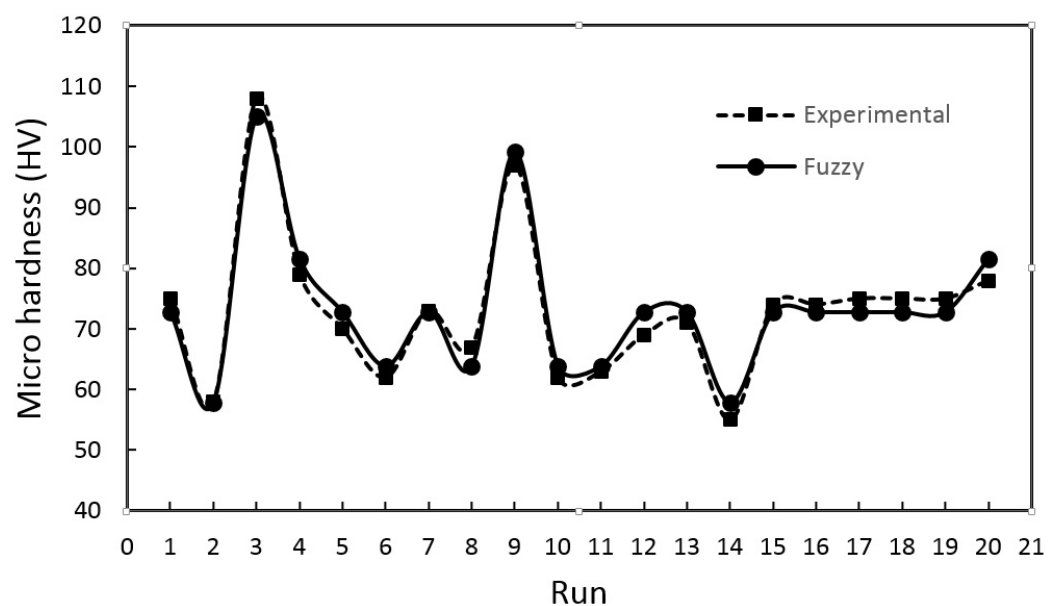


Figure 2. Micro-hardness and fuzzy micro-hardness results.

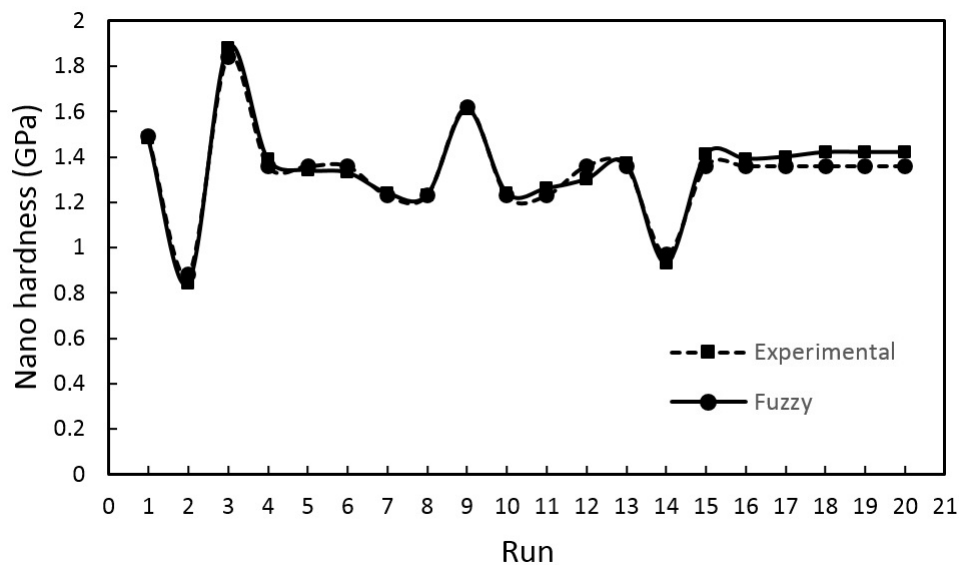


Figure 3. Nano-hardness and fuzzy nano-hardness results.

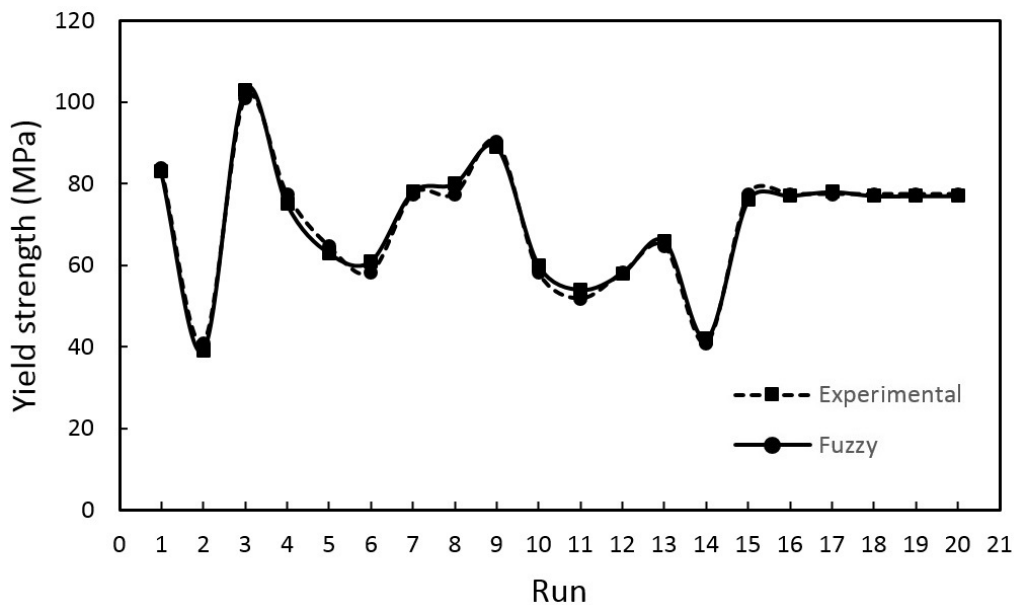


Figure 4. Yield strength and fuzzy yield strength results.

Table 3. The experimental and fuzzy predicted results.

Run	Micro-Hardness (HV)	Fuzzy Micro-Hardness (HV)	Nano-Hardness (GPa)	Fuzzy Nano-Hardness (GPa)	Yield Strength (MPa)	Fuzzy Yield Strength (MPa)
1	75	72.7	1.48	1.49	83	83.8
2	58	57.8	0.84	0.88	39	40.9
3	108	105	1.88	1.84	103	101
4	79	81.5	1.39	1.36	75	77.4
5	75	72.7	1.34	1.36	78	64.6

Table 3. Cont.

Run	Micro-Hardness (HV)	Fuzzy Micro-Hardness (HV)	Nano-Hardness (GPa)	Fuzzy Nano-Hardness (GPa)	Yield Strength (MPa)	Fuzzy Yield Strength (MPa)
6	62	63.8	1.33	1.36	61	58.2
7	70	72.7	1.24	1.23	63	77.4
8	67	63.8	1.23	1.23	80	77.4
9	97	99.2	1.61	1.62	89	90.2
10	62	63.8	1.24	1.23	60	58.2
11	63	63.8	1.26	1.23	54	51.8
12	69	72.7	1.3	1.36	58	58.2
13	71	72.7	1.37	1.36	66	64.6
14	55	57.8	0.93	0.97	42	40.9
15	74	72.7	1.41	1.36	76	77.4
16	74	72.7	1.39	1.36	77	77.4
17	75	72.7	1.4	1.36	78	77.4
18	75	72.7	1.42	1.36	77	77.4
19	75	72.7	1.42	1.36	77	77.4
20	78	81.5	1.42	1.36	77	77.4

Table 4 outlines the conditions used for optimization in the developed fuzzy logic model. According to the fuzzy logic model, the optimum condition (i.e., the highest strength) can be reached at the coded values of rotational speed, traverse speed, and axial force of -1.2 , 1.5 , and -0.46 , respectively. This means that the highest strength can be obtained using a tool rotational speed of 560 rpm, a tool traverse speed of 175 mm/min, and a tool axial force of 2.27 kN.

Table 4. The used condition for optimization of parameters.

Response	Goal	Lower	Target	Upper
Micro-hardness (HV)	Maximum	57.8	104	105
Nano-hardness (Gpa)	Maximum	0.88	1.85	1.84
Yield strength (Mpa)	Maximum	40.9	100	101

The typical macrostructure as well as the related microstructures of different areas of the welded sample are illustrated in Figure 5. It can be seen that the typical macrostructures of the FSWed joints consisted of three distinct zones, which included BM, thermomechanically affected zone (TMAZ), and SZ.

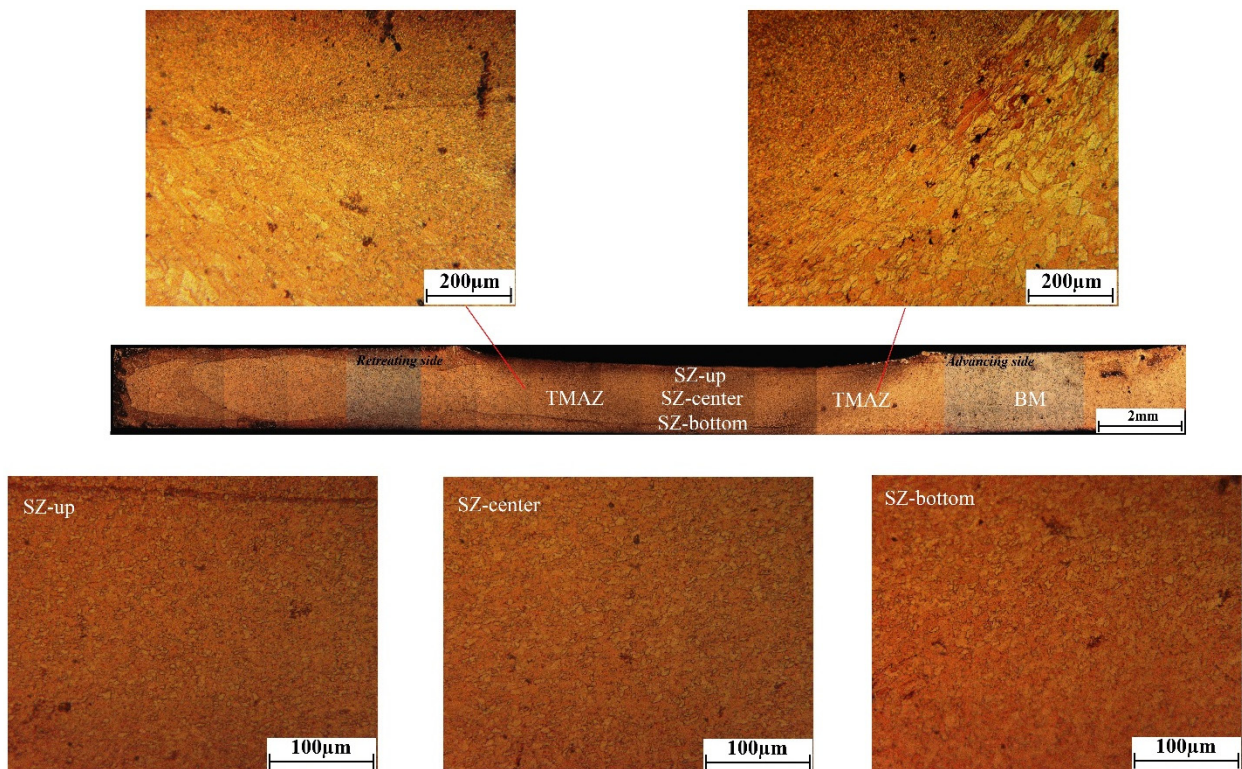


Figure 5. Typical macro-structure and related OM images of microstructural zones of the joints.

To compare the high- and low-heat input conditions, the samples of experiment numbers 2 (high heat input joints: coded as HH sample) and 5 (low heat input joints: coded as LH sample) were examined using OIM and TEM. The OIM maps, including inverse pole figure (IPF) map, grain boundary map, grain average misorientation (GAM) map, and Taylor factor map of the SZs of the HH and LH samples are shown in Figures 6 and 7, respectively.

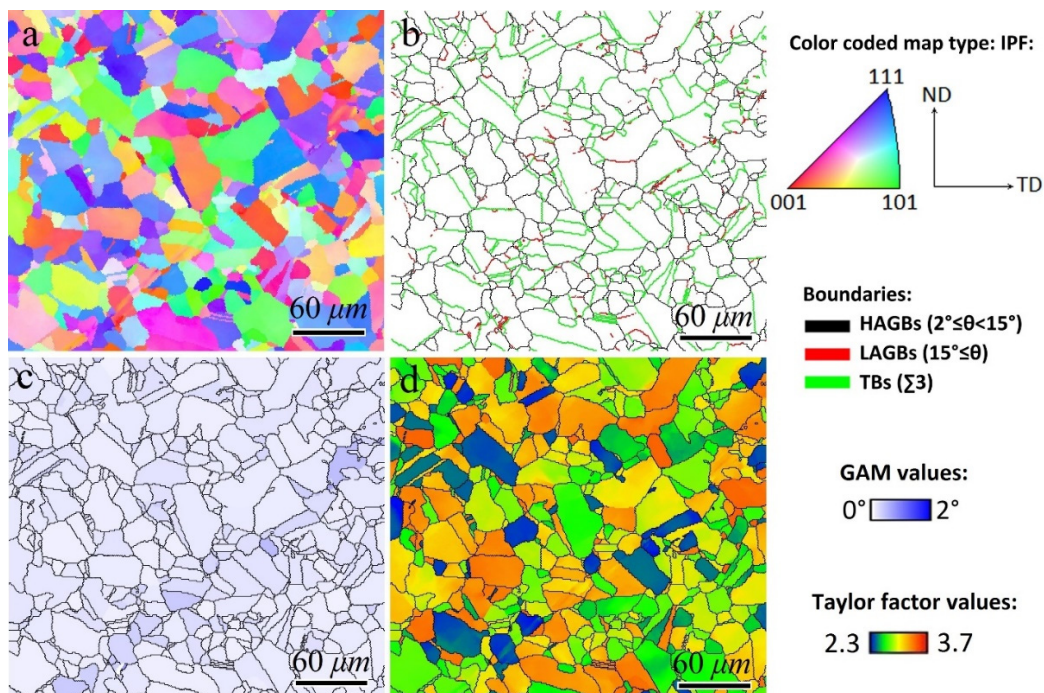


Figure 6. (a) IPF, (b) grain boundaries, (c) GAM, and (d) Taylor factor maps of the HH sample.

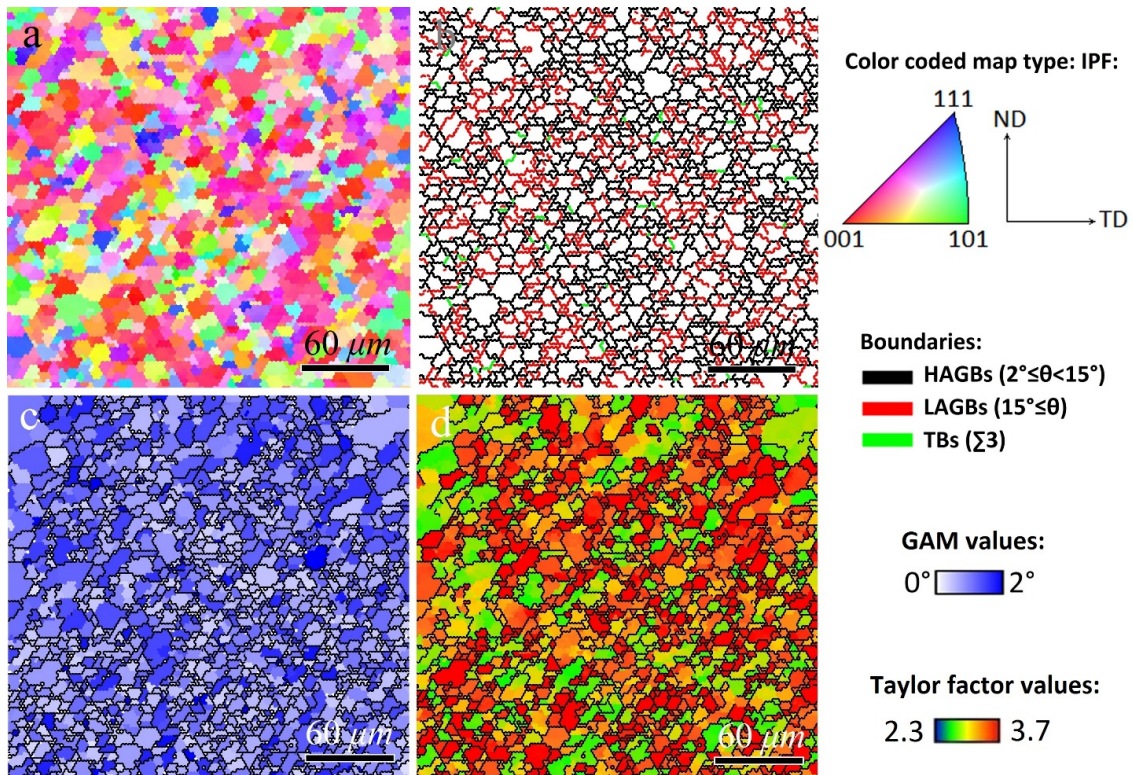


Figure 7. (a) IPF, (b) grain boundaries, (c) GAM, and (d) Taylor factor maps of the LH sample.

In addition, the quantitative data extracted from the EBSD analysis and the related peak temperatures measured during the FSW process are summarized in Table 5. To characterize the substructures (i.e., dislocation structure and density) of the HM and LM samples, TEM analysis was also carried out, and the corresponding results are illustrated in Figure 8. As can be seen, the dislocation structures appeared to be similar in both samples; however, the dislocation density in the LH sample was greater than that of the HH sample.

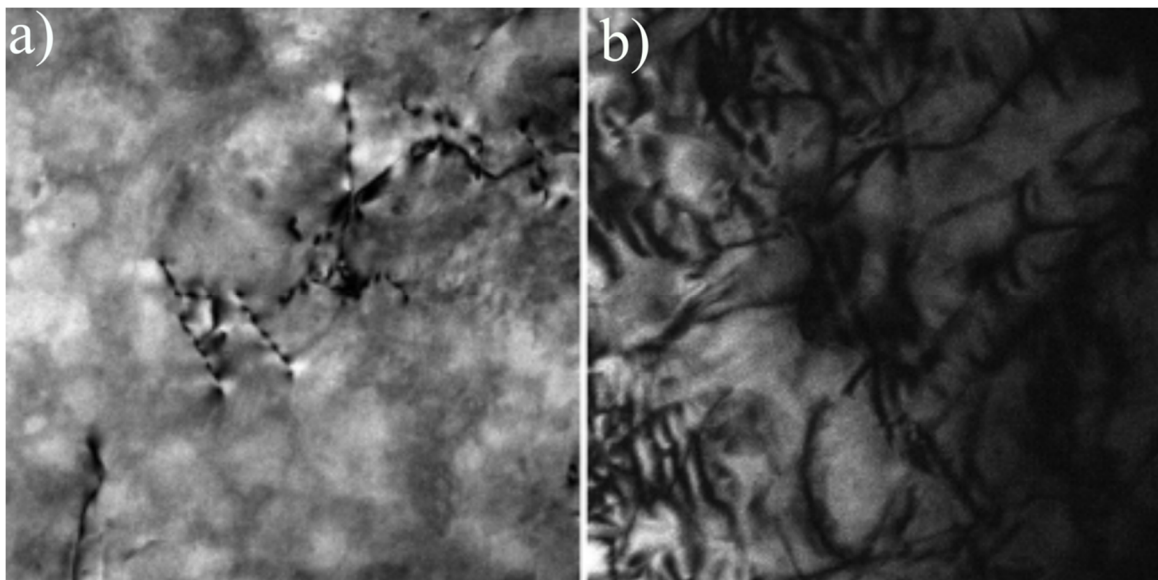


Figure 8. TEM images showing dislocation structures and densities in (a) HH sample, and (b) LH sample.

Table 5. EBSD data in conjunction with peak temperatures of the joints welded at the conditions of experiment numbers 2 (high heat input) and 5 (low heat input).

Sample	Grain Size (μm)	HAGB (mm)	Average GAM Value	Average Taylor Factor	Peak Temperature ($^{\circ}\text{C}$)
Run 2 (high heat input)	26.9	5.01	0.56	2.8	450
Run 5 (low heat input)	12.1	8.72	1.82	3.2	310

4. Discussion

The as-received BMs were in an annealed state, which consisted of a structure with large grains (average grain size of 39 μm) and annealing twins (as shown in Figure 5). In addition, as shown in Figure 5, the cross-sections of the joints were composed of BM, TMAZ, and SZ. As there was a gradient of strain and temperature from BM toward SZ during FSW, the different microstructural zones appeared in the cross-sections of the joints. BM is neither affected by the applied deformation nor by the heat that is induced via the rotational tool; hence, its microstructure does not change during FSW. In TMAZ, the material was affected by both parameters, the temperature and the applied deformation; however, neither the stored energy nor the temperature were usually high enough to drive for a full restoration (e.g., DRX) phenomenon. Consequently, the gains in TMAZ were mostly elongated along the shear direction induced by the rotational tool. On the other hand, in SZ, the temperature and the strain at the center of the joint could reach its maximum value; hence, the metallurgical restoration mechanisms could be completed during FSW. For instance, as shown in Figure 5, different areas of the SZ of the joint (i.e., top, middle, and bottom) experienced full DRX. The dynamic recrystallization during FSW of pure copper is usually driven by continuous and discontinuous DRX (CDRX and DDRX) through which fine and equiaxed grains with internal substructures are formed [5].

According to Table 3, the micro-hardness, nano-hardness, and yield strength of the LH sample (i.e., 75 HV, 1.34 GPa, and 78 MPa, respectively) were higher than those in the HH sample (i.e., 58 HV, 0.84 GPa, and 39 MPa, respectively). In addition, the hardness, nano-hardness, and yield strength profiles presented in Figures 2–4 indicated that they followed the same trend due to their similar physical and mechanical nature. These three mechanical properties stand for the strength of the joint. Thus, the difference between the mechanical properties of different joints (e.g., LH and HH samples) can be explained by strengthening mechanisms. During severe plastic deformation, the competing nature of the applied plastic strain and the generated frictional/deformation heat may cause microstructural restoration or work hardening [20,21].

The LH sample exhibited superior mechanical strength relative to HH. As outlined in Table 5, the peak temperature of LH (i.e., 310 $^{\circ}\text{C}$) was much lower than the peak temperature of HH (i.e., 450 $^{\circ}\text{C}$); thus, it was expected that the grain growth via DRX during FSW was more restricted in the LH sample relative to the HH one. This hypothesis is consistent with the results presented in Figures 6 and 7, which illustrate much finer grain size in the LH sample relative to the HH one. Needless to mention, according to the Hall–Petch relation ($\sigma_y = \sigma_0 + k_y g^{-1/2}$), the smaller the grain size, the higher the strength of a metal.

The density of the dislocations is another strengthening mechanism to be taken into account. According to the equation of ($\Delta\sigma_D = \alpha_1 G b \rho^{1/2}$) [22], the higher the dislocation densities, the more superior the strength, where $\Delta\sigma_D$ is the increased amount of strength by dislocation density, α_1 is constant, G is the shear modulus, b refers to the Burgers vector, and ρ belongs to the dislocation density. According to [23,24], the GAM maps, illustrated in Figures 6 and 7, can be considered as a qualitative estimation for internal energy or dislocation density. The higher the GAM value, the greater the dislocation densities. A comparison between Figures 6c and 7c reveals that the GAM value of the LH sample was

much higher than that of the HH sample, which was also confirmed by TEM micrographs (Figure 8).

The effect of texture is another strengthening mechanism that is often represented as the Taylor factor in the literature [25]. A comparison between Figures 6d and 7d indicates that the average value of the Taylor factor for the LH sample was much greater than that of the HH sample. The greater the Taylor factor, the higher the strength and the lower the strain hardening coefficients [26].

5. Conclusions

The developed fuzzy logic model well predicted the mechanical properties of FSWed copper joints. According to this model, the highest strength of the joints could be achieved when the tool rotational speed, tool traverse speed, and tool axial force are fixed at 560 rpm, 175 mm/min, and 2.27 kN, respectively. The low heat input joints, owing to the finer grain sizes, higher density of dislocations, and larger Taylor factors, indicated greater strength relative to the high input joints. Microstructure characterization revealed that the dominant strengthening mechanisms of the joints were dislocation density, texture effect, and grain-boundary hardening.

Author Contributions: M.J., Conceptualization, Methodology, Formal Analysis, Writing—Original Draft; A.H., Methodology, Investigation, Formal Analysis, Writing—Original Draft; R.V.B., Conceptualization, Methodology, Validation, Review and Editing; M.P., Conceptualization, Validation, Review and Editing; H.R.J., Conceptualization, Validation, Review and Editing. All authors have read and agreed to the published version of the manuscript.

Funding: This research received no external funding.

Institutional Review Board Statement: Not applicable.

Informed Consent Statement: Not applicable.

Data Availability Statement: Not applicable.

Conflicts of Interest: The authors declare no conflict of interest.

References

1. Davis, J.R. *Copper and Copper Alloys*; ASM International: Materials Park, OH, USA, 2001.
2. Heidarzadeh, A.; Saeid, T.; Klemm, V.; Chabok, A.; Pei, Y. Effect of Stacking Fault Energy on the Restoration Mechanisms and Mechanical Properties of Friction Stir Welded Copper Alloys. *Mater. Des.* **2019**, *162*, 185–197. [[CrossRef](#)]
3. Heidarzadeh, A.; Saeid, T. Correlation between Process Parameters, Grain Size and Hardness of Friction-Stir-Welded Cu–Zn Alloys. *Rare Met.* **2018**, *37*, 388–398. [[CrossRef](#)]
4. Mironov, S.; Inagaki, K.; Sato, Y.S.; Kokawa, H. Microstructural Evolution of Pure Copper During Friction-Stir Welding. *Philos. Mag.* **2015**, *95*, 367–381. [[CrossRef](#)]
5. Heidarzadeh, A.; Mironov, S.; Kaibyshev, R.; Çam, G.; Simar, A.; Gerlich, A.; Khodabakhshi, F.; Mostafaei, A.; Field, D.P.; Robson, J.D.; et al. Friction Stir Welding/Processing of Metals and Alloys: A Comprehensive Review on Microstructural Evolution. *Prog. Mater. Sci.* **2021**, *117*, 100752. [[CrossRef](#)]
6. Meng, X.; Huang, Y.; Cao, J.; Shen, J.; dos Santos, J.F. Recent Progress on Control Strategies for Inherent Issues in Friction Stir Welding. *Prog. Mater. Sci.* **2021**, *115*, 100706. [[CrossRef](#)]
7. Babu, S.R.; Hudgikar, S.R.K.; Sekhar, Y.P. Experimental Investigation on Friction Stir Welding of Hdpe Reinforced with Sic and Al and Taguchi-Based Optimization. In *Advances in Applied Mechanical Engineering*; Springer: Singapore, 2020. [[CrossRef](#)]
8. Kumar, D.; Kumar, J. Optimization of Parameters in Friction Stir Welding of Aa6101-T6 by Taguchi Approach. In *Advanced Engineering Optimization through Intelligent Techniques*; Springer: Singapore, 2020. [[CrossRef](#)]
9. Shunmugasundaram, M.; Kumar, A.P.; Sankar, L.P.; Sivasankar, S. Optimization of Process Parameters of Friction Stir Welded Dissimilar Aa6063 and Aa5052 Aluminum Alloys by Taguchi Technique. *Mater. Today Proc.* **2020**, *27*, 871–876. [[CrossRef](#)]
10. Dhabale, R.B.; Jatti, V.S. Experimental Study of Defects and Mechanical Properties During under-Water Friction Stir Welding of Al6061-6063 Alloys. In *Techno-Societal 2018*; Springer Nature: Cham, Switzerland, 2020. [[CrossRef](#)]
11. Ramesh, N.R.; Kumar, V.S. Experimental Erosion-Corrosion Analysis of Friction Stir Welding of Aa 5083 and Aa 6061 for Sub-Sea Applications. *Appl. Ocean Res.* **2020**, *98*, 102121. [[CrossRef](#)]
12. Heidarzadeh, A.; Javidani, M.; Mofarreh, M.; Farzaneh, A.; Chen, X. Submerged Dissimilar Friction Stir Welding of Aa6061 and Aa7075 Aluminum Alloys: Microstructure Characterization and Mechanical Property. *Metals* **2021**, *11*, 1592. [[CrossRef](#)]

13. Senthil, S.M.; Parameshwaran, R.; Nathan, S.R.; Kumar, M.B.; Deepandurai, K. A Multi-Objective Optimization of the Friction Stir Welding Process Using Rsm-Based-Desirability Function Approach for Joining Aluminum Alloy 6063-T6 Pipes. *Struct. Multidiscip. Optim.* **2020**, *62*, 1117–1133. [[CrossRef](#)]
14. Sasikumar, A.; Gopi, S.; Kumar, M.S.; Selvarajan, L. Predicting Tensile Strength of Filler Added Friction Stir Welded Aa6082 and Aa5052 Dissimilar Joint. *Mater. Today Proc.* **2020**, *46*, 9207–9211. [[CrossRef](#)]
15. Huang, Y.; Xie, Y.; Meng, X.; Li, J.; Zhou, L. Joint Formation Mechanism of High Depth-to-Width Ratio Friction Stir Welding. *J. Mater. Sci. Technol.* **2019**, *35*, 1261–1269. [[CrossRef](#)]
16. Huang, Y.; Xie, Y.; Meng, X.; Lv, Z.; Cao, J. Numerical Design of High Depth-to-Width Ratio Friction Stir Welding. *J. Mater. Processing Technol.* **2018**, *252*, 233–241. [[CrossRef](#)]
17. Heidarzadeh, A.; Testik, Ö.M.; Gülerüz, G.; Barenji, R.V. Development of a Fuzzy Logic Based Model to Elucidate the Effect of Fsw Parameters on the Ultimate Tensile Strength and Elongation of Pure Copper Joints. *J. Manuf. Processes* **2020**, *53*, 250–259. [[CrossRef](#)]
18. Eren, B.; Guvenc, M.A.; Mistikoglu, S. Artificial Intelligence Applications for Friction Stir Welding: A Review. *Met. Mater. Int.* **2021**, *27*, 193–219. [[CrossRef](#)]
19. Dao, M.; Chollacoop, N.; Van Vliet, K.J.; Venkatesh, T.A.; Suresh, S. Computational Modeling of the Forward and Reverse Problems in Instrumented Sharp Indentation. *Acta Mater.* **2001**, *49*, 3899–3918. [[CrossRef](#)]
20. Xie, Y.; Meng, X.; Chang, Y.; Mao, D.; Yang, Y.; Xu, Y.; Wan, L.; Huang, Y. Ameliorating Strength-Ductility Efficiency of Graphene Nanoplatelet-Reinforced Aluminum Composites Via Deformation-Driven Metallurgy. *Compos. Sci. Technol.* **2022**, *219*, 109225. [[CrossRef](#)]
21. Xie, Y.; Meng, X.; Li, Y.; Mao, D.; Wan, L.; Huang, Y. Insight into Ultra-Refined Grains of Aluminum Matrix Composites Via Deformation-Driven Metallurgy. *Compos. Commun.* **2021**, *26*, 100776. [[CrossRef](#)]
22. Zuiko, I.; Kaibyshev, R. Deformation Structures and Strengthening Mechanisms in an Al-Cu Alloy Subjected to Extensive Cold Rolling. *Mater. Sci. Eng. A* **2017**, *702*, 53–64. [[CrossRef](#)]
23. Tian, Y.Z.; Gao, S.; Zhao, L.J.; Lu, S.; Pippan, R.; Zhang, Z.F.; Tsuji, N. Remarkable Transitions of Yield Behavior and Lüders Deformation in Pure Cu by Changing Grain Sizes. *Scr. Mater.* **2018**, *142*, 88–91. [[CrossRef](#)]
24. Heidarzadeh, A. Tensile Behavior, Microstructure, and Substructure of the Friction Stir Welded 70/30 Brass Joints: Rsm, Ebsd, and Tem Study. *Arch. Civ. Mech. Eng.* **2019**, *19*, 137–146. [[CrossRef](#)]
25. Starink, M.J.; Deschamps, A.; Wang, S.C. The Strength of Friction Stir Welded and Friction Stir Processed Aluminium Alloys. *Scr. Mater.* **2008**, *58*, 377–382. [[CrossRef](#)]
26. Heidarzadeh, A.; Laleh, H.M.; Gerami, H.; Hosseinpour, P.; Shabestari, M.J.; Bahari, R. The Origin of Different Microstructural and Strengthening Mechanisms of Copper and Brass in Their Dissimilar Friction Stir Welded Joint. *Mater. Sci. Eng. A* **2018**, *735*, 336–342. [[CrossRef](#)]